Hydrothermal synthesis and structures of the homoleptic iodate complexes $[M(IO_3)_6]^{2-}$ (M = Mo, Zr)

Thomas C. Shehee, Stephen F. Pehler, Thomas E. Albrecht-Schmitt*

Department of Chemistry, 179 Chemistry Building, Auburn University, Auburn, AL 36849, USA

Abstract

$Rb_2[Mo(IO_3)_6]$ (**1**), $Rb_2[Zr(IO_3)_6]$ (**2**), and $Cs_2[Zr(IO_3)_6]$ (**3**) have been prepared under hydrothermal conditions. These compounds are isostructural and consist of alkali metal cations and isolated $[M(IO_3)_6]^{2-}$ anions containing transition metals in +4 oxidation state. The $[M(IO_3)_6]^{2-}$ anions possess $\bar{3}$ symmetry with the transition metal centers residing on $\bar{3}$ sites. The iodate anions ligate the transition metals through a single oxygen atom. All of the iodate oxygen atoms form long interactions with the alkali metal cations. These interactions result in a contraction of the O−M−O bond angles along a single three-fold axis. Crystallographic data (193 K): **1**, trigonal, space group $R\bar{3}$, $a =$ 11.4048(8) Å, $c = 11.4062(8)$ Å, $Z = 3$, Mo Kα, $\lambda = 0.71073$, $R(F) = 2.52\%$ for 43 parameters with 711 reflections with $I > 2\sigma(I)$; **2**, trigonal, space group $R\bar{3}$, $a = 11.5575(9)$ Å, $c = 11.4987(9)$ Å, $Z = 3$, Mo Kα, $\lambda = 0.71073$, $R(F) = 2.16\%$ for 43 parameters with 742 reflections with $I > 2\sigma(I)$; **3**, trigonal, space group $R\bar{3}$, $a = 11.768(1)$ Å, $c = 11.720(1)$ Å, $Z = 3$, Mo Kα, $\lambda = 0.71073$, $R(F) = 1.61\%$ for 43 parameters with 781 reflections with $I > 2\sigma(I)$.
© 2004 Elsevier B.V. All rights reserved.

1. Introduction

Transition metal iodates have been the subject of substantial interest for almost three decades. Initial studies emphasized the crystal growth of compounds with polar structures in an effort to deduce structure-property relationships, e.g. piezo- and pyroelectric coefficients [1–3], second-harmonic generation [2,4–6], and magnetism [4,7]. While many hydrated transition metal iodates are centrosymmetric [8], most anhydrous transition metal iodates are noncentrosymmetric; examples of which include $Co(IO_3)_2$ [4], β-$Ni(IO_3)_2$ [9], α-$Cu(IO_3)_2$ [2,10], and $Zn(IO_3)_2$ [9]. The magnetic properties of some transition metal iodates have proven to be quite rich, with antiferromagnetic ordering being observed for $Fe(IO_3)_3$ below $T_N = 17$ K, and weak ferromagnetism being found for $Ni(IO_3)_2 \cdot 2H_2O$ beneath 3 K [4]. More recently $Zn(IO_3)_2 \cdot 2H_2O$, $Ni(IO_3)_2 \cdot 2H_2O$, and $M(IO_3)_2 \cdot 4H_2O$ (M = Ni, Co) have been the subject of single crystal Raman and

IR spectroscopic studies allowing for complete assignment of iodate stretching and bending modes [9,11–13].

The crystal chemistry of transition metal iodates is dominated by the formation of extended structures owing to the commonly bridging nature of the iodate anion. While some systems are truly low-dimensional (e.g. $NaCu(IO_3)_3$ [14]), many adopt three-dimensional network structures. Molecular systems are surprisingly rare, being known only from the chromyl iodate anion $[CrO_3(IO_3)]^{1-}$ [15] and from $[MoO_2(IO_3)_4]^{2-}$ [16]. Herein we report the preparation and crystal structures of three zero-dimensional, or molecular, transition metal iodates, $Rb_2[Mo(IO_3)_6]$ (**1**), $Rb_2[Zr(IO_3)_6]$ (**2**), and $Cs_2[Zr(IO_3)_6]$ (**3**).

2. Experimental

2.1. Syntheses

MoO_3 (99.95%, Alfa-Aesar), I_2O_5 (98%, Alfa-Aesar), H_5IO_6 (99%, Alfa-Aesar), HIO_3 (99.5%, Alfa-Aesar), KCl

---

* Corresponding author. Tel.: +1 334 844 6983; fax: +1 334 844 6959.
E-mail address: albreth@auburn.edu (T.E. Albrecht-Schmitt).

Table 1
Crystallographic data for Rb$_2$[Mo(IO$_3$)$_6$] (**1**), Rb$_2$[Zr(IO$_3$)$_6$] (**2**), Cs$_2$[Zr(IO$_3$)$_6$] (**3**)

Formula	Rb$_2$[Mo(IO$_3$)$_6$] (**1**)	Rb$_2$[Zr(IO$_3$)$_6$] (**2**)	Cs$_2$[Zr(IO$_3$)$_6$] (**3**)
Formula mass (amu)	1316.28	1311.56	1406.44
Color and habit	Orange rhombohedron	Colorless rhombohedron	Colorless rhombohedron
Crystal system	Trigonal	Trigonal	Trigonal
Space group	$R\bar{3}$ (No. 148)	$R\bar{3}$ (No. 148)	$R\bar{3}$ (No. 148)
a (Å)	11.4048(8)	11.5575(9)	11.768(1)
c (Å)	11.4062(8)	11.4987(9)	11.720(1)
V (Å^3)	1284.8(2)	1330.17(18)	1405.7(3)
Z	3	3	3
T (°C)	−80	−80	−80
λ (Å)	0.71073	0.71073	0.71073
ρ_{calcd} (g cm^{-3})	5.104	4.912	4.984
μ(Mo Kα) (cm^{-1})	173.17	166.07	143.83
$R(F)$ for $F_o^2 > 2\sigma(F_o^2)$[a]	0.0252	0.0216	0.0161
$R_w(F_o^2)$[b]	0.0577	0.0443	0.0407

[a] $R(F) = \sum ||F_o| - |F_c||/ \sum |F_o|$.

[b] $R_w(F_o^2) = \left[\sum [w(F_o^2 - F_c^2)^2]/ \sum wF_o^4 \right]^{1/2}$.

(99.94%, Fisher), ZrOCl$_2$ (99.9%, Alfa-Aesar), Rb$_2$CO$_3$ (99%, Alfa-Aesar), and Cs$_2$CO$_3$ (99%, Alfa-Aesar) were used as received. RbIO$_4$ and CsIO$_4$ were prepared from the reaction of Rb$_2$CO$_3$ or Cs$_2$CO$_3$ with H$_5$IO$_6$. Distilled and millipore filtered water with a resistance of 18.2 MΩ cm was used in all reactions. Reactions were run in Parr 4749 23 mL autoclaves with PTFE liners for 3d at 200 °C and cooled at a rate of 9 °C/h to 23 °C. SEM/EDX analyses were performed using a JEOL 840/Link Isis instrument. K, Rb, Cs, Mo, Zr, and I percentages were calibrated against standards.

2.2. Rb$_2$Mo(IO$_3$)$_6$ (**1**)

MoO$_3$ (86 mg, 0.597 mmol), H$_5$IO$_6$ (274 mg, 1.202 mmol), and Rb$_2$CO$_3$ (139 mg, 0.602 mmol) were loaded in a 23 mL PTFE-lined autoclave. Water (1.0 mL) was then added to the solids. The product consisted of orange rhombohedral crystals of Rb$_2$Mo(IO$_3$)$_6$ (**1**) in trace amounts, with the major product being pale yellow rods of RbMoO$_3$(IO$_3$) [17]. The mother liquor was decanted from the crystals, which were then washed with water and methanol, and allowed to dry.

2.3. Rb$_2$Zr(IO$_3$)$_6$ (**2**)

RbIO$_4$ (229 mg, 0.829 mmol), I$_2$O$_5$ (138 mg, 0.414 mmol), and ZrOCl$_2$ (133 mg, 0.425 mmol) were loaded in a 23 mL PTFE-lined autoclave. Water (1.5 mL) was then added to the solids. The product consisted of colorless rhombohedral crystals of Rb$_2$Zr(IO$_3$)$_6$ (**2**) dispersed in ZrO$_2$ powder. The mother liquor was decanted from the crystals, which were then washed with water and methanol, and allowed to dry. Yield 2, 56 mg (10% yield based on Zr). EDX analysis for Rb$_2$Zr(IO$_3$)$_6$ provided a Rb:Zr:I ratio of 2:1:6.

2.4. Cs$_2$Zr(IO$_3$)$_6$ (**3**)

CsIO$_4$ (250 mg, 0.772 mmol), I$_2$O$_5$ (127 mg, 0.380 mmol), and ZrOCl$_2$ (123 mg, 0.382 mmol) were loaded in a 23-mL PTFE-lined autoclave. Water (1.5 mL) was then added to the solids. The product consisted of colorless rhombohedral crystals of Cs$_2$Zr(IO$_3$)$_6$ (**3**) dispersed in ZrO$_2$ powder. Yield 3, 54 mg (10% yield based on Zr). EDX analysis for Cs$_2$Zr(IO$_3$)$_6$ provided a Cs:Zr:I ratio of 2:1:6.

2.5. Crystallographic studies

Single crystals of Rb$_2$[Mo(IO$_3$)$_6$] (**1**), Rb$_2$[Zr(IO$_3$)$_6$] (**2**), and Cs$_2$[Zr(IO$_3$)$_6$] (**3**) were mounted on a glass fibers with epoxy and aligned on a Bruker SMART APEX CCD X-ray diffractometer with a digital camera. An Oxford Cryostat was used to adjust the data collection temperature to −80 °C. Intensity measurements were performed using graphite monochromated Mo Kα radiation from a sealed tube with a monocapillary collimator. SMART was used to determine the preliminary cell constants from 90 frames collected with an exposure time of 10 s, and to subsequently control the data collection. For **1**–**3**, the intensities of reflections of a

Table 2
Atomic coordinates and equivalent isotropic displacement parameters for Rb$_2$[Mo(IO$_3$)$_6$] (**1**)

Atom	x	y	z	U_{eq} (Å^2)[a]
Rb(1)	0	0	0.8331(1)	0.016(1)
Mo(1)	2/3	1/3	5/6	0.012(1)
I(1)	0.4075(1)	0.0208(1)	0.7245(1)	0.014(1)
O(1)	0.5779(4)	0.1775(4)	0.7266(3)	0.018(1)
O(2)	0.4591(4)	−0.0644(4)	0.6223(3)	0.021(1)
O(3)	0.4295(4)	−0.0441(4)	0.8616(3)	0.019(1)

[a] U_{eq} is defined as one-third of the trace of the orthogonalized **U**$_{ij}$ tensor.

Table 3
Atomic coordinates and equivalent isotropic displacement parameters for
Rb$_2$[Zr(IO$_3$)$_6$] (**2**)

Atom	x	y	z	U_{eq} (Å^2)[a]
Rb(1)	0	0	0.83508(7)	0.0142(2)
Zr(1)	2/3	1/3	5/6	0.0081(2)
I(1)	0.39520(3)	0.38101(3)	0.72004(2)	0.0089(1)
O(1)	0.5528(3)	0.3772(3)	0.7223(3)	0.0121(7)
O(2)	0.4501(3)	0.5180(3)	0.6205(3)	0.0137(7)
O(3)	0.4252(3)	0.4668(3)	0.8574(3)	0.0151(7)

[a] U_{eq} is defined as one-third of the trace of the orthogonalized $\mathbf{U}_{ij}$ tensor.

sphere were collected by a combination of three sets of exposures (frames). Each set had a different ϕ angle for the crystal and each exposure covered a range of 0.3° in ω. A total of 1800 frames were collected with an exposure time per frame of 30 s.

Determination of integrated intensities and global cell refinement were performed with the Bruker SAINT (v 6.02) software package using a narrow-frame integration algorithm. An analytical absorption correction was applied, followed by a semi-empirical absorption correction using SADABS [18]. The program suite SHELXTL (v 5.1) was used for space group determination (XPREP), structure solution (XS), and refinement (XL) [19]. The final refinement included anisotropic displacement parameters for all atoms and a secondary extinction parameter. Some crystallographic details are listed in Table 1 for **1**–**3**. Atomic coordinates and equivalent isotropic displacement parameters are given in Tables 2–4 for **1**, **2**, and **3**, respectively.

3. Results and discussion

3.1. Syntheses

Rb$_2$[Mo(IO$_3$)$_6$] (**1**) is only isolated in trace quantities from syntheses that were originally employed to prepare RbMoO$_3$(IO$_3$) [17]. While Cs$_2$[Zr(IO$_3$)$_6$] (**3**) can be prepared from the reaction of CsIO$_4$ with ZrO$_2$ at 425 °C in supercritical water, this reaction yields only trace amounts of Cs$_2$[Zr(IO$_3$)$_6$] (**3**) in the form of minute crystals (<0.01 mm on an edge). Instead, it was observed that **3** could be prepared in low yield, from the reaction of CsIO$_4$ with I$_2$O$_5$ and ZrOCl$_2$ under mild hydrothermal conditions. A similar reac-

Table 4
Atomic coordinates and equivalent isotropic displacement parameters for
Cs$_2$[Zr(IO$_3$)$_6$] (**3**)

Atom	x	y	z	U_{eq} (Å^2)[a]
Cs(1)	0	0	0.8386(1)	0.013(1)
Zr(1)	2/3	1/3	5/6	0.008(1)
I(1)	0.3973(1)	0.0191(1)	0.7220(1)	0.009(1)
O(1)	0.4559(2)	−0.0596(2)	0.6279(2)	0.016(1)
O(2)	0.5486(2)	0.1811(2)	0.7244(2)	0.014(1)
O(3)	0.4235(2)	−0.0344(2)	0.8584(2)	0.017(1)

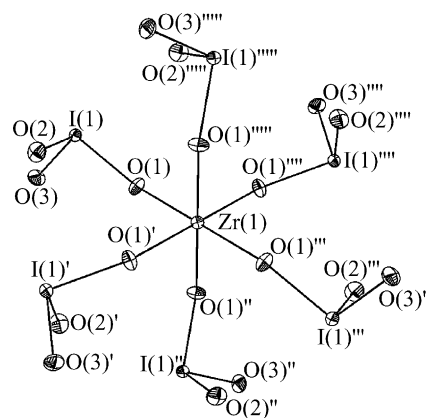[a] U_{eq} is defined as one-third of the trace of the orthogonalized $\mathbf{U}_{ij}$ tensor.

Fig. 1. A depiction of the [Zr(IO$_3$)$_6$]$^{2-}$ anion in Cs$_2$[Zr(IO$_3$)$_6$] (**3**) (50% probability ellipsoids are shown).

tion where RbIO$_4$ was substituted for CsIO$_4$ was also used to produce the Rb (**2**) analog of **3**. Crystals of the K$^+$ salt of [Zr(IO$_3$)$_6$]$^{2-}$ can also be grown under mild hydrothermal conditions. However, these crystals are too small for single crystal X-ray diffraction measurements.

3.2. Structures of Rb$_2$[Mo(IO$_3$)$_6$] (**1**), Rb$_2$[Zr(IO$_3$)$_6$] (**2**), and Cs$_2$[Zr(IO$_3$)$_6$] (**3**)

Compounds **1**–**3** are isostructural and all crystallize in the trigonal space group $R\bar{3}$. The compounds consist of isolated alkali metal cations and [M(IO$_3$)$_6$]$^{2-}$ (M = Mo, Zr) anions. The geometry around the transition metal centers in the [M(IO$_3$)$_6$]$^{2-}$ anions are best described as a slightly distorted octahedron, and each metal resides on a $\bar{3}$ site, resulting in a single unique M−O bond length for each compound. A view of the [Zr(IO$_3$)$_6$]$^{2-}$ anion from **3**, which is also representative of **1** and **2**, is shown in Fig. 1. The Mo−O and Zr−O bond lengths are 1.967(4), 2.070(3), and 2.069(2) Å, for **1**, **2**, and **3**, respectively. Selected bond distances are given in Table 5. Using the Zr−O bond lengths, the bond-valence sums for Zr in **2** and **3** were calculated to be 4.19 and 4.20, respectively, which are consistent with Zr(IV) [20,21].

In each compound there is likely a symmetric elongation of the M−O bonds along a single three-fold axis that is observed in the O−M−O bond angles being distorted from orthogonality by 4.30(16)°, 4.05(13)°, and 4.10(9)° in **1**, **2**,

Table 5
Selected bond distances (Å) for Rb$_2$[Mo(IO$_3$)$_6$] (**1**), Rb$_2$[Zr(IO$_3$)$_6$] (**2**), and
Cs$_2$[Zr(IO$_3$)$_6$] (**3**)

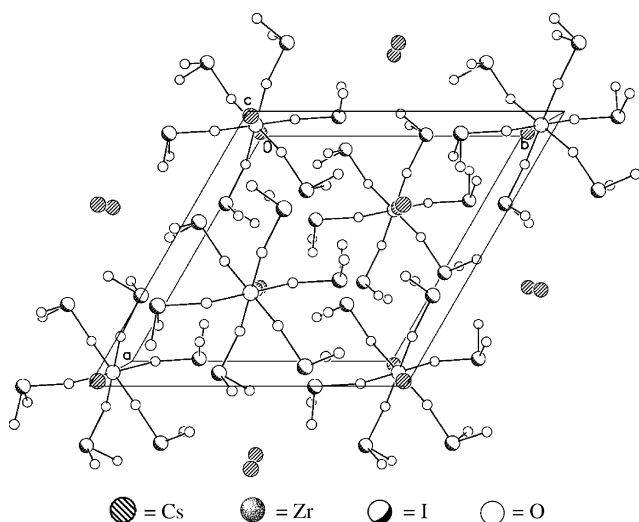|			
Rb$_2$[Mo(IO$_3$)$_6$] (1)			
Mo(1)−O(1) (x 6)	1.967(4)	I(1)−O(2)	1.795(4)
I(1)−O(1)	1.870(4)	I(1)−O(3)	1.800(4)
Rb$_2$[Zr(IO$_3$)$_6$] (2)			
Zr(1)−O(1) (x 6)	2.070(3)	I(1)−O(2)	1.793(3)
I(1)−O(1)	1.844(3)	I(1)−O(3)	1.804(3)
Cs$_2$[Zr(IO$_3$)$_6$] (3)			
Zr(1)−O(1) (x 6)	2.069(2)	I(1)−O(2)	1.785(2)
I(1)−O(1)	1.847(2)	I(1)−O(3)	1.800(2)

= Cs ◉ = Zr ◑ = I ◯ = O

Fig. 2. A view of the packing in $Cs_2[Zr(IO_3)_6]$ (**3**).

and **3**, respectively. As a d^2 ion Mo(IV) might be expected to exhibit Jahn-Teller distortions that could potentially result in this distortion. However, Zr(IV), being d^0, would not be expected to show the same type of distortion, although a second-order Jahn-Teller distortion is possible [22–30]. An examination of the packing of the alkali metal cations and the $[M(IO_3)_6]^{2-}$ anions reveals that there are short interactions between the iodate oxygen atoms that bind the transition metal centers and the alkali metal cations. The length of these interactions increases from Rb^+ to Cs^+, and ranges from 2.927(4) to 3.008(4) Å in **1**, 2.994(3) to 3.048(3) Å in **2**, and 3.143(2) to 3.146(2) Å in **3**. It is likely that the interactions between these ion-pairs are the cause of the small deviations from idealized octahedral symmetry. A packing diagram for **3** is shown in Fig. 2. The I–O bond distances show expected trends where the terminal oxygen atoms have shorter bond lengths than those that bind the transition metal centers. In the case of the **3**, the terminal distances are 1.785(2) and 1.800(2) Å, whereas the bridging distance is 1.847(2) Å.

4. Conclusions

This work has provided the first evidence for the stabilization of Mo(IV) by iodate, which has previously only been found with Mo(VI) (16,17). Assignment of the formal oxidation state for Mo can be made with some confidence given that $Rb_2[Mo(IO_3)_6]$ (**1**) is isostructural with $Rb_2[Zr(IO_3)_6]$ (**2**) and $Cs_2[Zr(IO_3)_6]$ (**3**) where the oxidation state of the transition metal can be unambiguously assigned. The M–O bond distances also show an expected shortening from Zr to Mo. These compounds may also provide molecular precursors to extended structures containing octahedral transition metal iodate units, which will be the subject of future reports.

5. Auxiliary material

Further details of the crystal structure investigation may be obtained from the Fachinformationzentrum Karlsruhe, D-76344 Eggenstein-Leopoldshafen, Germany (fax: +49 7247 808 666; e-mail: crysdata@fiz-karlsruhe.de) on quoting depository numbers CSD 413880, 414091, and 413881.

References

[1] R. Liminga, S.C. Abrahams, J. Appl. Crystallogr. 9 (1976) 42.
[2] R. Liminga, S.C. Abrahams, J.L. Bernstein, J. Chem. Phys. 62 (1975) 4388.
[3] C. Svensson, S.C. Abrahams, J.L. Bernstein, J. Solid State Chem. 36 (1981) 195.
[4] S.C. Abrahams, R.C. Sherwood, J.L. Bernstein, K. Nassau, J. Solid State Chem. 7 (1973) 205.
[5] S.C. Abrahams, R.C. Sherwood, J.L. Bernstein, K. Nassau, J. Solid State Chem. 7 (1973) 274.
[6] M. Jansen, J. Solid State Chem. 17 (1976) 1.
[7] S.C. Abrahams, J.L. Bernstein, J.B.A.A. Elemans, G.C. Verschoor, J. Chem. Phys. 59 (1973) 2007.
[8] J.B.A.A. Elemans, G.C. Verschoor, J. Inorg. Nucl. Chem. 35 (1973) 3183.
[9] S. Peter, G. Pracht, N. Lange, H.D. Lutz, Z. Anorg. Allg. Chem. 626 (2000) 208.
[10] R. Liminga, S.C. Abrahams, J. Appl. Crystallogr. 9 (1976) 42.
[11] G. Pracht, N. Lange, H.D. Lutz, Thermochim. Acta 293 (1997) 13.
[12] G. Pracht, R. Nagel, E. Suchanek, N. Lange, H.D. Lutz, Z. Anorg. Allg. Chem. 624 (1998) 1355.
[13] V. Schellenschläger, G. Pracht, H.D. Lutz, J. Raman Spectr. 32 (2001) 373.
[14] P.K.S. Gupta, S. Ghose, E.O. Schlemper, Z. Krystallogr. 181 (1987) 167.
[15] P. Loefgren, Acta Chem. Scand. 21 (1967) 2781.
[16] R.E. Sykora, D.M. Wells, T.E. Albrecht-Schmitt, J. Solid State Chem. 166 (2002) 442.
[17] R.E. Sykora, K.M. Ok, P.S. Halasyamani, T.E. Albrecht-Schmitt, J. Am. Chem. Soc. 124 (2002) 1951.
[18] SADABS 2001, Program for absorption correction using SMART CCD based on the method of Blessing: R.H. Blessing, Acta Crystallogr. A 51 (1995) 33.
[19] G.M. Sheldrick, SHELXTL PC, Version 6.12, An Integrated System for Solving, Refining, and Displaying Crystal Structures from Diffraction Data; Siemens Analytical X-Ray Instruments, Inc.: Madison, WI 2001.
[20] I.D. Brown, D. Altermatt, Acta Crystallogr. B 41 (1985) 244.
[21] N.E. Brese, M. O'Keeffe, Acta Crystallogr. B47 (1991) 192.
[22] U. Opik, M.H.L. Pryce, Proc. R. Soc. (London) A 161 (1937) 220.
[23] R.A. Wheeler, M.H. Whangbo, T. Hughbanks, R. Hoffman, J.K. Burdett, T.A. Albright, J. Am. Chem. Soc. 108 (1986) 2222.
[24] R.G. Pearson, J. Mol. Struct. 103 (1983) 25.

[25] S.K. Kang, H. Tang, T.A. Albright, J. Am. Chem. Soc. 115 (1993) 1971.
[26] R.E. Cohen, Nature 358 (1992) 136.
[27] J.K. Burdett, Molecular Shapes, Wiley-Interscience, New York, 1980.
[28] M. Kunz, I.D. Brown, J. Solid State Chem. 115 (1995) 395.
[29] J.B. Goodenough, J.M. Longo, Crystallographic and magnetic properties of perovskite and perovskite-related compounds, in: K.H. Hellwege, A.M. Hellwege (Eds.), Landolt-Bornstein, vol. 4, Springer-Verlag, Berlin, 1970, pp. 126–314.
[30] I.D. Brown, Acta Crystallogr. B 33 (1977) 1305.